Nuclear Instruments and Methods in Physics Research A 648 (2011) 46–51

Contents lists available at ScienceDirect

Nuclear Instruments and Methods in Physics Research A

journal homepage: www.elsevier.com/locate/nima

Challenging measurement of the $^{16}O+^{27}Al$ elastic and inelastic angular distributions up to large angles

M. Cavallaro [a,*], F. Cappuzzello [a,b], D. Carbone [a,b], A. Cunsolo [a,b], A. Foti [b,c], R. Linares [d], D. Pereira [e], J.R.B. Oliveira [e], P.R.S. Gomes [d], J. Lubian [d], R. Chen [f]

[a] INFN, Laboratori Nazionali del Sud, Via S. Sofia 62, I-95125 Catania, Italy
[b] Dipartimento di Fisica e Astronomia, Università di Catania, Via S. Sofia 64, I-95125 Catania, Italy
[c] INFN, Sezione di Catania, Via S. Sofia 64, I-95125 Catania, Italy
[d] Instituto de Física, Universidade Federal Fluminense, Litoranea s/n, Gragoatá, Niterói, Rio de Janeiro 24210-340, Brazil
[e] Universidade de São Paulo, Departamento de Física Nuclear, Instituto de Física da Universidade de São Paulo, Caixa Postal 66318, 05315-970 São Paulo, SP, Brazil
[f] Institute of Modern Physics, CAS, Lanzhou, PR China

ARTICLE INFO

Article history:
Received 25 February 2011
Received in revised form
11 April 2011
Accepted 26 April 2011
Available online 19 May 2011

Keywords:
Elastic scattering
Magnetic spectrometers
Trajectory reconstruction

ABSTRACT

The $^{16}O+^{27}Al$ elastic and inelastic angular distributions have been measured in a broad angular range ($13^\circ < \theta_{lab} < 52^\circ$) at about 100 MeV incident energy. The use of the MAGNEX large acceptance magnetic spectrometer and of the ray-reconstruction analysis technique has been crucial in order to provide, in the same experiment, high-resolution energy spectra and cross-section measurements distributed over more than seven orders of magnitude down to hundreds of nb/sr.

1. Introduction

Recently [1] rainbow-like structures have been theoretically predicted in the elastic channel for heavy ions systems such as $^{16}O+^{27}Al$ and $^{16}O+^{58}Ni$ by a new generation of parameter free coupled channel calculations using the São Paulo potential [2] and the Glauber model [3]. These results, obtained at energies several times the Coulomb barrier, are unexpected due to the high absorption that should be present in such heavy system collisions.

The rainbow pattern has been experimentally well established for lighter systems like $\alpha+$nucleus, $^{12}C+^{12}C$, $^{16}O+^{12}C$ and $^{16}O+^{16}O$, the heaviest system that so far has shown a prominent refractive structure in the elastic channel. An excellent topical review including a complete bibliography on this subject has been recently published by Khoa et al. [4]. It is important to point out that tremendous efforts have been done in order to reveal the rainbow structures, since at large scattering angles the elastic cross-sections become extremely small ($d\sigma/d\omega \sim 100$ nb/sr and less). In such conditions, guaranteeing a reasonable signal to noise ratio in the measured spectra could represent a major problem. Moreover, supplementary difficulties arise for heavy systems scattering, resulting in stringent requirements as listed below:

(1) The overlap between events from elastic and from other reaction channels must be avoided, which means that satisfactory ion identification is demanded.
(2) The typically small excitation energy of the first excited states in heavy targets makes the separation between the elastic and inelastic channels much more challenging compared to lighter systems. In this case, a high energy resolution is required, which has a direct influence on the choice of the target thickness, due to the emphasized role of the energy straggling in heavy systems. Thus, a difficult compromise between energy resolution and statistical significance of the collected data must be found.
(3) The discrimination between the scattering events of interest and those from the target contaminants could be rather difficult especially at backward angles, where the inelastic scattering on the contaminants can be dominant (order of magnitude bigger).
(4) High angular resolution is required to characterize the rainbow structures and distinguish between the refractive and the diffractive natures of the oscillation patterns. The heavier is the system the more rapid are the oscillations and consequently the higher is the necessary resolution.

* Corresponding author. Tel.: +39 0 95 542 384.
E-mail address: manuela.cavallaro@lns.infn.it (M. Cavallaro).

0168-9002/
doi:10.1016/j.nima.2011.04.042

(5) Similarly, a higher angular accuracy is necessary for heavier systems, since the exact location of the minima in the angular distributions is fundamental to test different theoretical approaches against the experimental data.
(6) The typical count rates in heavy ions experiments are smaller than light ones, due to more severe constraints in the target thickness and in the availability of intense beams. In this context, a large angular acceptance is needed to allow for statistically significant data especially at large angles.

All of these complications are expected in the experimental study of the $^{16}O+^{27}Al$ elastic scattering and this explains the lack of experimental data for this process at sufficient backward angles. In this paper we illustrate the experimental technique and the data analysis method used to perform such an experiment and to extract energy spectra and angular distributions. It is based on the use of the MAGNEX large acceptance spectrometer for the detection of the ^{16}O ejectiles at the focal plane, and on the implementation of a high-performing algebraic ray-reconstruction technique. It will be demonstrated that the above listed experimental requirements are fulfilled by MAGNEX, which proves to be well suitable for this challenging experiment.

2. The experiment

MAGNEX is a quadrupole–dipole magnetic spectrometer installed at INFN–LNS (Italy), characterized by a large angular (≈ 50 mr) and momentum (-14.3%, $+10.3\%$) acceptance [5–7]. The $^{16}O^{8+}$ beam, delivered by the Tandem Van der Graaff accelerator at 99.2 MeV total incident energy, was focused on a ^{27}Al self-supporting target located in the MAGNEX scattering chamber. The elastically and inelastically scattered ^{16}O ions have been momentum analyzed by the spectrometer and detected by its Focal Plane Detector (FPD) [8–10].

A system of diaphragms was used in order to limit the beam spot size and the angular divergence at the target to 1.2 mm × 0.8 mr in the horizontal direction and 2.3 mm × 3 mr in the vertical one. In such conditions, the contribution of the beam divergence to the overall energy spreading is less than 50 keV at backward angles. Particular care has been taken in aligning the diaphragm system to guarantee that the beam intercepts the target along the spectrometer optical axis, thus getting the best resolution. More precisely, an accuracy of ± 0.1 mm in the definition of the spectrometer object point and ± 0.05 mr in the beam direction has been achieved.

As stated in the previous section, the choice of the target thickness was the result of a careful compromise between energy resolution and reaction yield constraints. In fact the experiment should provide a complete separation of the elastic channel from the first inelastic excitation of the ^{27}Al at 844 keV, still getting a reasonable count rate at backward angles, where the predicted cross-sections fall down. For this reason two different aluminum target foils have been mounted for the runs at different scattering angles, (i) a 100 μg/cm^2 target for the runs at forward angles ($13^\circ < \theta_{lab} < 36^\circ$) and (ii) a 137 μg/cm^2 one for the runs at backward angles ($31^\circ < \theta_{lab} < 52^\circ$). The uncertainty on the target thickness is about 10%.

The sources of energy spreading must be considered carefully to achieve the best energy resolution in the energy spectra. The use of the Tandem Van der Graaff accelerator guarantees a good monochromatic beam (≈ 10 keV). In this condition, the leading contribution to the overall energy widening comes from the kinematic broadening and from the energy straggling in the target. The former is particularly important for large scattering angles θ_{lab}. As an example, it produces an energy broadening of about 250 keV for the $^{27}Al(^{16}O, ^{16}O)^{27}Al$ reaction at 100 MeV incident energy, considering an angular resolution of 0.2° at $\theta_{lab}=50^\circ$.

A set of simulations was performed at different experimental conditions to estimate the energy straggling in the target. The energy loss straggling was predicted using a Monte Carlo procedure. First, the scattering position in the target was sorted randomly. Then, the energy loss of the beam up to that point was calculated considering the stopping power predicted from the SRIM code [11]. At this point, the scattering energy at a given angle was calculated and the energy loss of the scattered particle up to the backside of the target was deduced. One thousand events were sorted and the energy loss straggling was extracted from the Full Width at half Maximum (FWHM) of this final energy distribution. A plot of the obtained energy loss straggling for different target thicknesses is shown in Fig. 1, supposing a scattering angle $\theta_{lab}=50^\circ$ and a tilt of the target ladder $\theta_{target}=20^\circ$ around the vertical axis in the same direction of the spectrometer rotation.

In the different experimental runs, the optical axis of the spectrometer was centered at the laboratory angles $\theta_{opt}=18^\circ$, 24°, 29°, 35°, 41° and 46°. In all the runs the ejectiles trajectory were accepted between -5.2° and $+6.3^\circ$ in the horizontal direction and $\pm 7.0^\circ$ in the vertical, with respect to the optical axis. In such a way an angular overlap of about 6° between two contiguous sets of measurements was available.

Simulations were also performed considering different rotation angles of the target ladder θ_{target}. The energy straggling was calculated as a function of θ_{target} for different scattering angles as shown in Fig. 2.

According to the results of the simulations, it was decided to rotate the target ladder of $\theta_{target}=20^\circ$ in all the runs at different scattering angles. This allowed to minimize the spreading due to the sensibly different energy loss between the incident ^{16}O ions and those emitted at lower kinetic energy in the reaction.

The beam intensity was about 10 pnA for the runs at backward angles, being reduced down to 0.6 pnA at $\theta_{opt}=18^\circ$ to avoid distortions in the FPD response due to the high rate. A graphite Faraday cup (4 cm deep) having a circular aperture (8 mm diameter) and an electron suppression ring was used to stop the beam. A low noise circuit including a digital integrator was used to determine the collected charge with an intrinsic accuracy better than 0.5%. For each run, a quick on-line data reduction allowed to know the integrated charge in order that the recorded dataset was statistically

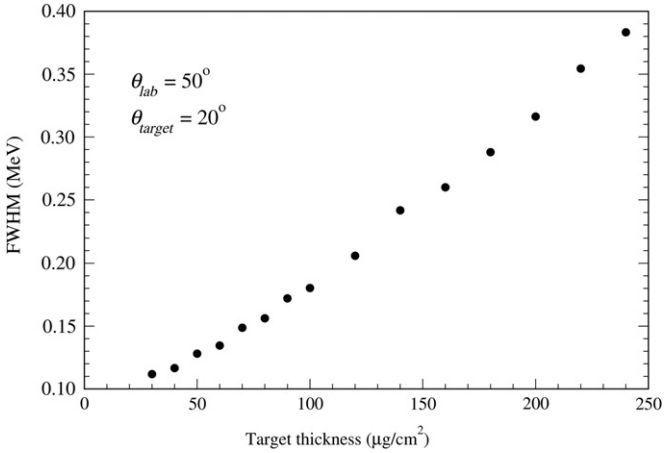

Fig. 1. Calculated energy straggling as a function of the target thickness for the $^{16}O+^{27}Al$ elastic scattering at 99.2 MeV, $\theta_{lab}=50^\circ$ and $\theta_{target}=20^\circ$. The calculation does not include the effect of the angular resolution. See text for the details of the simulation.

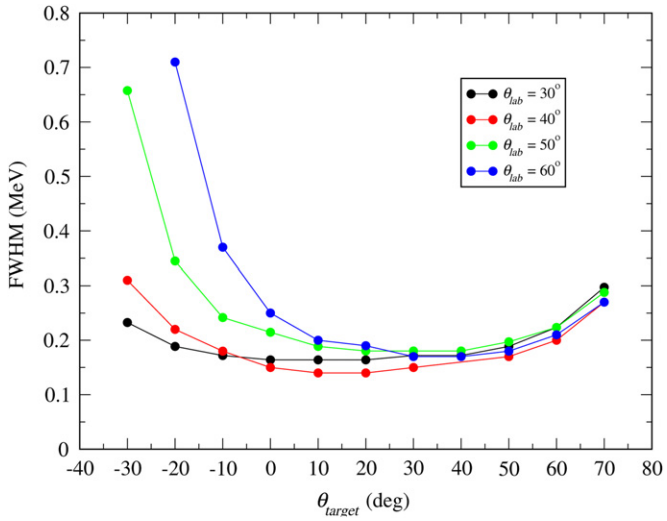

Fig. 2. Expected energy straggling as a function of the target rotation angle for different scattering angles: $\theta_{lab}=30^\circ$ (black), $\theta_{lab}=40^\circ$ (red), $\theta_{lab}=50^\circ$ (green), $\theta_{lab}=60^\circ$ (blue). (For interpretation of the references to color in this figure legend, the reader is referred to the web version of this article.)

significant even for the weakest channels (the inelastic at 844 keV at forward angles, the elastic at backward).

The magnetic fields of the MAGNEX quadrupole and dipole were tuned in order to transmit the scattered $^{16}O^{8+}$. The different reaction ejectiles within the spectrometer acceptance were momentum analyzed and focused on the FPD. For each angular setting the vertical focus was optimized for the momenta corresponding to the elastic channel.

The MAGNEX FPD is a hybrid gas detector with an array of 54 silicon pad detectors (70×50 mm^2 area, 500 μm thickness) at the back [8–10]. The FPD was filled with 99.95% pure is butane at 7 mbar pressure. A voltage of -1100 V was applied to the cathode resulting in a reduced electric field of about 7.8 V cm^{-1} mbar^{-1} for the drift region. The multiplication wires were supplied with $+750$ V in order to maintain a proportional regime with a gain factor of about 200. The silicon detectors were biased with $+50$ V to get a full depletion of their active volume. In such working conditions the FPD allows to cleanly identify the detected ions in atomic (Z) and mass (A) number and electric charge (q), and to precisely measure the horizontal and vertical impact positions (x_f, y_f) and direction (θ_f, ϕ_f) of the ions trajectory in the focal plane. Precise alignments were done in order to relate the parameters measured by the FPD to the spectrometer absolute reference frame, where the transport operators are defined. The sensitive elements of the detector (anodic strips, cathode, Frisch grid, and field shaping wires) have been simultaneously sighted with specially designed pin–pot of the magnets by means of bubble levels and theodolits. An overall accuracy better than 0.1 mm has been achieved in both the horizontal and vertical positionings of the FPD.

The use of a latching scaler module allowed the measurement of the ratio between the number of triggers and the number of the events treated by the acquisition system, thus providing a coefficient which accounts for the actual acquisition dead-time.

3. Data reduction and analysis

3.1. Transport map

The first step of the MAGNEX data reduction procedure is to build a transport map that describes the evolution of the phase-space parameters from the target point to the focal plane. In a schematic representation of a magnetic dispersive spectrometer, the initial coordinates $\mathbf{Q_i}=(\theta_i, y_i, \varphi_i, \delta)$ are connected to the final ones $\mathbf{Q_f}=(x_f, \theta_f, y_f, \varphi_f)$ by a relation

$$G : \mathbf{Q_i} \rightarrow \mathbf{Q_f} \tag{1}$$

where θ_i and φ_i are the horizontal and vertical angles, y_i is the vertical coordinate and $\delta=(p-p_0)/p_0$ is the fractional momentum deviation, being p the ion momentum and p_0 the reference one [12]. The final parameters x_f, y_f, θ_f, φ_f are the horizontal and vertical coordinates and angles of the ions in a plane normal to the reference trajectory. The function G describes a non-linear transport map, characteristic of the particular optical system, and simulates the response of the spectrometer.

As already discussed in recent publications [13,14], in the MAGNEX case, Eq. (1) is solved by an algebraic technique based on the formalism of differential algebra [15,16] implemented in the COSY INFINITY program [17]. Such a technique allows to calculate the map up to high order without long ray-tracing procedures. In addition it makes possible to invert the transport equations in order to get the initial coordinates $\mathbf{Q_i}$ from the measured final ones $\mathbf{Q_f}$. The initial parameters extracted from the solution of the inverse equation are directly related to the physical quantities of interest in a typical nuclear reaction analysis, as the modulus of the ion momentum and the scattering angle.

3.2. Ion identification

A precise reconstruction of the ions kinetic energy is one of the ingredients of an innovative technique to identify the reaction ejectiles crossing the spectrometer, as described in detail in Ref. [18]. Such technique is based on a standard $\Delta E-E$ method for the Z identification with a resolution $\Delta Z/Z=1/48$. Mass identification is achieved thanks to the simultaneous measurement of the kinetic energy T and the reconstructed fractional momentum δ of the detected ions. In Ref. [18], it has been shown that this technique allows to obtain a clear identification of the detected ions with a mass resolution as high as $\Delta A/A=1/160$. Since the measured horizontal position x_f at the focal plane is directly connected to the reconstructed δ of the ejectiles and the measured residual energy E_r is related to the kinetic energy T, when a high mass resolution is not necessary, the identification can be also achieved by relating the x_f and E_r parameters [8].

An example of identification plots is shown in Fig. 3 for the $^{16}O+^{27}Al$ experiment at $\theta_{opt}=24^\circ$. In particular, Fig. 3(a) shows the energy loss ΔE measured by one of the FPD proportional wires against the residual energy E_r measured by the silicon detectors. The ΔE parameter is corrected for the length of the ion trajectory along the active region of the FPD. Due to the large angular range spanned by the trajectories entering in the FPD ($40^\circ<\theta_f<72^\circ$), such lengths $l(\theta_f)$ are quite different depending on the angle θ_f. Since the energy loss signals need to be compared at a fixed length, this in turns requires the measurement of the angle θ_f. Fig. 3(b) shows a plot of x_f against E_r for the oxygen isotopes selected in the $\Delta E-E_r$ plot.

3.3. Parameters at the focal plane

Once the $^{16}O^{8+}$ ejectiles are selected, the measured horizontal and vertical positions and angles at the focal plane are analyzed. A bi-dimensional histogram of the measured θ_f versus x_f for the experimental setting at $\theta_{opt}=18^\circ$ ($13^\circ<\theta_{lab}<21^\circ$) is shown in Fig. 4. Since the FPD is inclined by 59.2° (1.033 rad) with respect to the plane perpendicular to the optical axis [19], the measured θ_f are distributed around that angle in the plot. In abscissa, $x_f=0$

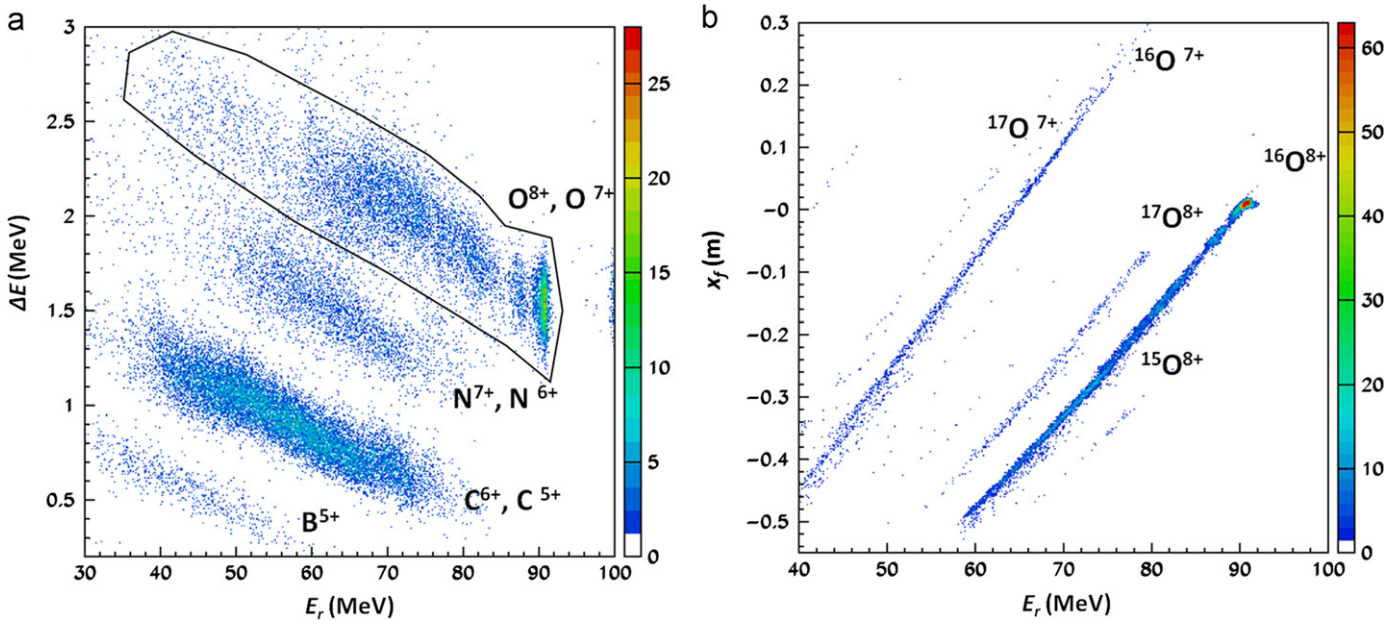

Fig. 3. Two-dimensional spectra measured in the $^{16}O+^{27}Al$ reaction at 99.2 MeV and scattering angle $19^\circ < \theta_{lab} < 30^\circ$. Panel (a) shows the $\Delta E - E_r$ plot, where the ΔE parameter is corrected for the angle of the detected ions. The observed oxygen ions group is circled with a contour line. Panel (b) shows the $x_f - E_r$ plot for the selected oxygen isotopes.

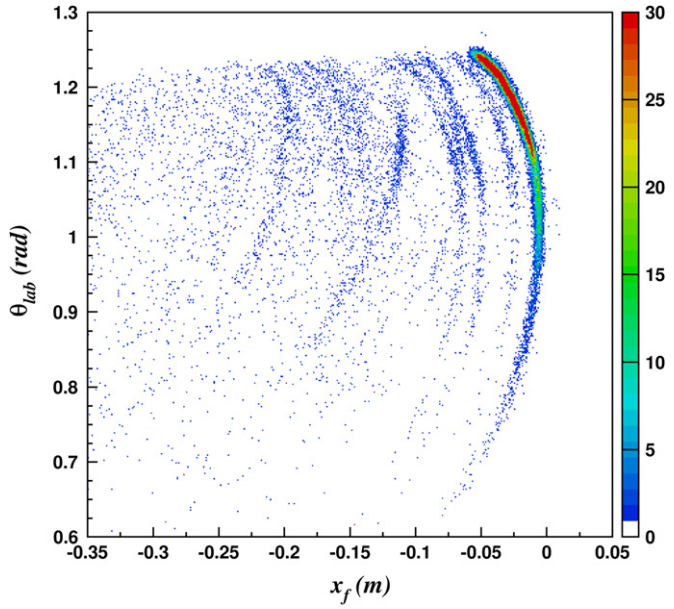

Fig. 4. Plot of the horizontal angle against the horizontal position measured at the focal plane for the $^{16}O^{8+}$ ejectiles of the $^{27}Al(^{16}O, ^{16}O)^{27}Al$ reaction at 99.2 MeV and $13^\circ < \theta_{lab} < 21^\circ$.

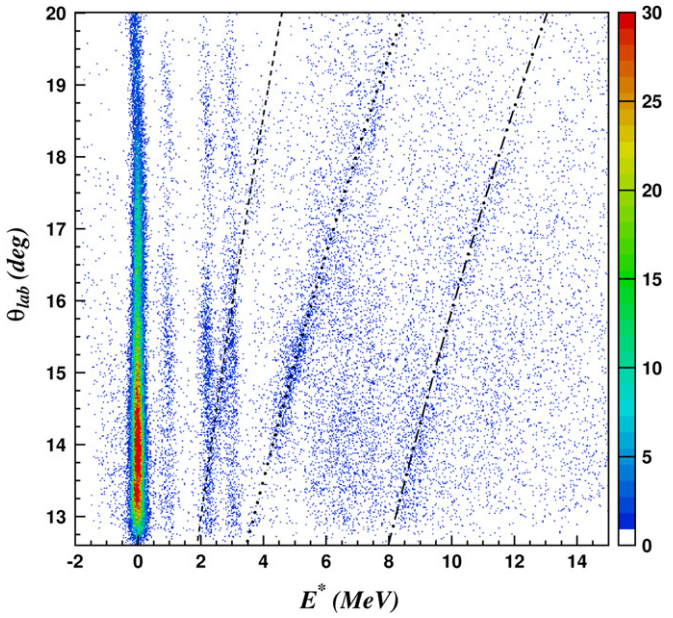

Fig. 5. Two-dimensional plot of the reconstructed θ_{lab} against the ^{27}Al apparent excitation energy E^* for the $^{27}Al(^{16}O, ^{16}O)^{27}Al$ reaction at 99.2 MeV and $\theta_{opt}=18^\circ$. The lines represent the calculated kinematics for the population of the ^{16}O (dashed) and ^{12}C ground (dotted) and the ^{12}C excited state at 4.439 MeV (dot-dashed).

corresponds to the trajectories in the optical axis. The well correlated loci in the plot indicate the population of the ground (at about $x_f=0$) and of the excited states of ^{27}Al. The curvature of the loci is due both to the kinematic effect and to the aberrations in the horizontal phase space. It is also distinguishable, with different curvatures, the population of the states of ^{12}C and ^{16}O due to target impurities, that will be commented in the following.

3.4. Reconstructed parameters

The ray-reconstruction algorithms have been used to build the transport map to 10th order. In the COSY INFINITY input, the geometry of the spectrometer (distances between the magnetic elements, length of the drift spaces, and slits defining the solid angle) and the size and location of the FPD are set as the experimental ones. The dipole and quadrupole magnetic strengths have been measured by probes with an overall uncertainty of about $\pm 0.1\%$ (this value includes the uncertainty in the probes position). The three-dimensional field shapes are described as Enge functions [20] obtained from interpolations of measured data, which account for the shape of the effective boundaries by 5th order polynomials [21–24].

Fig. 5 shows an example of reconstructed parameters for the $^{16}O^{8+}$ reaction ejectiles. In particular the scattering angle θ_{lab} is shown against the ^{27}Al apparent excitation energy E^*, which is defined as the excitation energy of the ^{27}Al reaction products, assuming a binary process. The ^{27}Al ground and several excited states are well visible as vertical and straight loci, as expected since the E^* parameter is not depending on the scattering angle for transitions to the ^{27}Al states. The tilted loci represent the events relative to the presence of ^{16}O and ^{12}C contaminants in the target that induce the population of the ^{16}O and ^{12}C ground and ^{12}C excited state at 4.439 MeV. The distinct curvatures are due to the different kinematics of ^{16}O scattering on the ^{16}O and ^{12}C target nuclei. This helps the identification and discrimination of such events, which is one of the qualifying features of the ray-reconstruction technique implemented in MAGNEX, meeting one of the key requirements listed in the introduction of this paper.

An average resolution of about 200 keV is obtained in the explored phase space, allowing a clean separation of the elastic from the inelastic channels. One can also notice the different counts distributions due to the different shapes of the angular distribution between the elastic and the inelastic transitions. In particular, those relative to the states at 0.844, 1.014, 2.212, 2.735 and 2.982 MeV show a very similar oscillating pattern, with a well defined minimum at around $\theta_{lab}=17^\circ$. It is the expected behavior, since all of those belong to the same $L=2$ multiplet ^{28}Si(2^+) $\otimes$ $\nu(1d_{5/2})^{-1}$ [25,26]. The analysis of the kinematic lines shown in Fig. 5 does allow a further check of the accuracy in the reconstruction of the experimental laboratory angle θ_{lab}. As an example, the crossing point of the ^{27}Al (^{16}O, ^{16}O) ^{27}Al$_{2.212}$ inelastic locus with the ^{16}O+^{16}O elastic one depends only on the laboratory angle, once the beam energy is known. The discrepancy between the kinematic predictions and the experimental data is within 0.1°. This is in agreement with the recently published results with the MAGNEX spectrometer in similar experimental conditions [18].

A projection of the data on the excitation energy axis provides a more quantitative comparison of the different channel yields. Some examples of energy spectra are shown in Fig. 6 at $18.0^\circ < \theta_{lab} < 19.0^\circ$ and $42.7^\circ < \theta_{lab} < 46.4^\circ$. The differential cross-section in the forward angle range has been estimated to be about 37 mb/sr, while it decrease to about 780 nb/sr in average in the shown backward angles range. Smaller values up to few hundreds of nb/sr are measured at further backward angles. Despite the many orders of magnitude differences in the elastic cross-sections, the obtained spectra present essentially the same features with similar resolution and acceptable signal to noise ratio. In particular the first inelastic peaks (0.844+1.015 MeV) are still well distinguishable from the

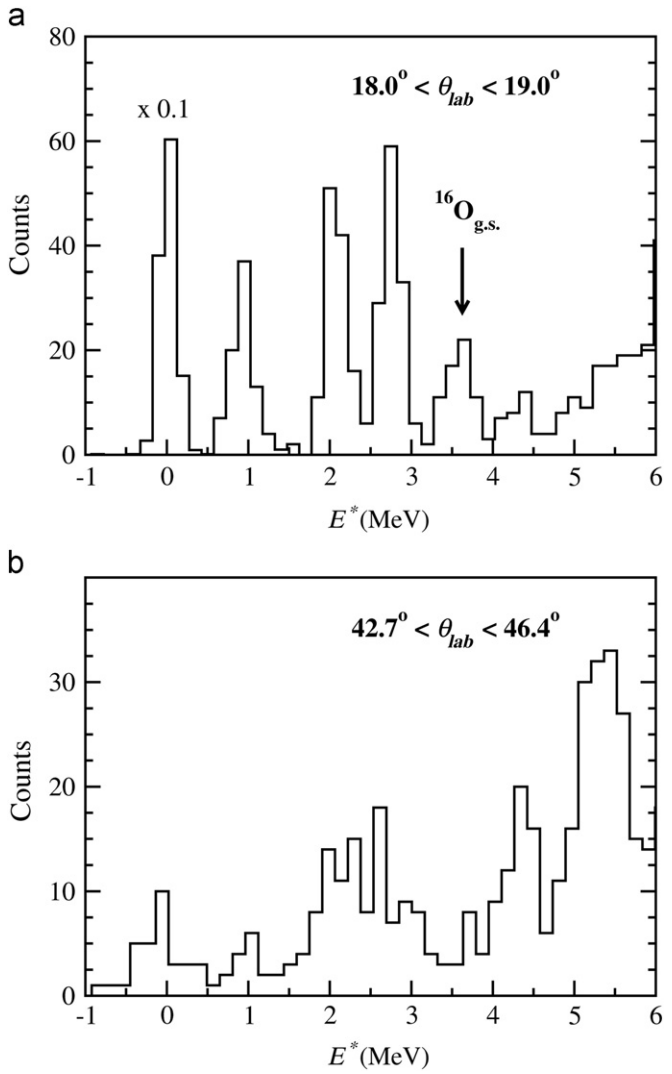

Fig. 6. ^{27}Al apparent excitation energy spectra for two different scattering angles: (a) $18.0^\circ < \theta_{lab} < 19.0^\circ$, (b) $42.7^\circ < \theta_{lab} < 46.4^\circ$. The peak relative to the ^{27}Al$_{g.s.}$ in the plot (a) has been scaled by a factor 0.1. The peak marked with an arrow refers to the ^{16}O+^{16}O elastic scattering.

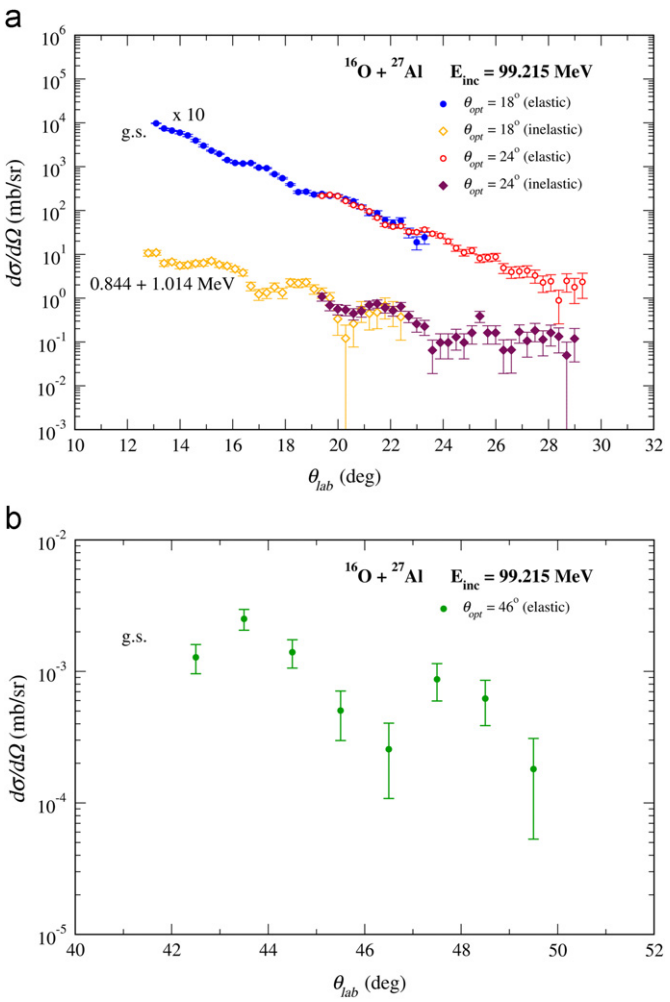

Fig. 7. Angular distributions of the differential cross-section in the laboratory reference frame. Upper panel: for the ^{16}O+^{27}Al elastic and sum of the first two target excitation at 0.844 and 1.014 MeV and $\theta_{opt}=18^\circ$ and 24°. Lower panel: for the ^{16}O+^{27}Al elastic at $\theta_{opt}=46^\circ$.

elastic one. This is a major achievement of this challenging experiment.

The angular distributions of the absolute cross-section have been deduced for the transition to the ^{27}Al ground and unresolved excited states at 0.844 and 1.014 MeV. The results for the experimental runs at $\theta_{opt}=18^\circ$, 24° and 46° are shown in Fig. 7. The differential solid angle for the full spectrometer acceptance has been carefully determined taking into account the overall transport efficiency as described in Ref. [14]. A dead-time coefficient of about 15% has been measured. An angular bin of 0.3° has been chosen for the dataset at $\theta_{opt}=18^\circ$ and 24° and of 1° at $\theta_{opt}=46^\circ$ in order to achieve a good compromise between the statistical uncertainties in the number of counts for each bin and the angular resolution. The error bars include both a statistical contribution (between about 1% at forward angles and 50% at the backward ones) and a component due to the uncertainty in the solid angle determination (about 3%). An overall systematic error of about 10% is estimated, mainly due to the uncertainties on the target thickness. A more detailed analysis of the errors in the differential cross-section has been done in Ref. [14].

Thanks to the large angular acceptance of the spectrometer, significant overlaps between the two measurements at adjacent angles $\theta_{opt}=18^\circ$ and 24° are available, thus allowing a supplementary check of the quality of the absolute measurement of the cross-section. The observed agreement in the overlap region is excellent both in the elastic and inelastic channels. In addition, the achieved angular resolution is estimated to be within 0.3° at $\theta_{opt}=18^\circ$, with slightly poorer results in the run at $\theta_{opt}=24^\circ$ and 46° likely due to worse experimental conditions. The systematic error on θ_{lab} has been evaluated to be 0.3° based on the cross-points of kinematic lines referring to different reactions, as for example those shown in Fig. 5. This is in agreement to what found for the spectrometer in similar conditions [13] and it is good enough to safely determine the minima of the angular distribution oscillation. All of this confirms the reliability of the instrument for this kind of studies.

4. Conclusions

The ^{16}O+^{27}Al elastic and inelastic scattering has been successfully measured at 99.2 MeV incident energy using the MAGNEX spectrometer. The reaction ejectiles have been detected at forward and at backward angles up to $\theta_{lab}=52^\circ$, corresponding to $\theta_{CM}=80^\circ$ in the center of mass reference frame. All the challenging requirements of the experiment have been satisfied, allowing to clearly identify the ^{16}O ions, to separate the ground from the first excited states of ^{27}Al at 844 keV and to measure accurate absolute cross-sections and angular distributions even at backward angles.

We emphasize that the cross-section decreases of about 7 order of magnitude in the explored angular region, down to about 100 nb/sr. A detailed analysis of the physical implications and of the motivations supporting this study is not the goal of the present paper and will be discussed in a forthcoming publication. Nevertheless, the accomplishment of such results is an encouraging issue opening new perspectives in particular in the understanding of the fascinating research of nuclear rainbow with heavy ions [4] and more generally in the study of heavy-ion processes [27–30].

The described technique is in fact general enough to be easily applied to many other systems in a broad energy range. In this view the relevant point is the separation capability between the elastic and the inelastic channels. As a consequence, the choice of the bombarding energy and the target thickness should be carefully evaluated. In fact, since the energy resolution of a magnetic spectrometer is a relative quantity (about 1/1000 of the ions kinetic energy in the case of MAGNEX) the obtained FWHM of the peaks increases linearly with the bombarding energy. As an example, simulations for the ^{16}O+^{27}Al reaction at backward angles, assuming the same performances of the spectrometer (energy and angular resolution), show that the upper limit for the total incident energy is about 300 MeV mainly due to the kinematic broadening. For higher energies the first excited state is not separable from the ground. The requirements on the energy resolution become less stringent if dealing with even–even systems, where the first excited state is typically at higher excitation energy. For heavier targets, a smaller kinematic broadening is present, which normally balance the worse energy straggling. For example we estimate that similar experimental achievements can be obtained with nickel even targets.

References

[1] D. Pereira, et al., Phys. Lett. B 670 (2009) 330.
[2] L.C. Chamon, et al., Phys. Rev. C 66 (2002) 014610.
[3] M.S. Hussein, R.A. Rego, C.A. Bertulani, Phys. Rep. 201 (1991) 279.
[4] D.T. Khoa, et al., J. Phys. G: Nucl. Part. Phys. 34 (2007) R111.
[5] A. Cunsolo, et al., Nucl. Instr. and Meth. A 481 (2002) 48.
[6] A. Cunsolo, et al., Eur. Phys. J.—Spec. Topics 150 (2007) 343.
[7] M. Cavallaro, et al., AIP Conf. Proc. 1224 (2010) 112.
[8] M. Cavallaro, First Application of the MAGNEX spectrometer: investigation of the ^{19}F(^{7}Li,^{7}Be)^{19}O reaction at 52.2 MeV, Ph.D. Thesis, University of Catania, 2008.
[9] C. Boiano, et al., IEEE Trans. Nucl. Sci. NS-55 (2008) 3563.
[10] M. Cavallaro et al., Nucl. Instr. and Meth. A, in preparation.
[11] J.F. Ziegler, et al., Nucl. Instr. And Meth. B 268 (2010) 1818.
[12] D.C. Carey, Optics of Charged-Particle Beams, Chur, Harwood, 1987.
[13] F. Cappuzzello, et al., Nucl. Instr. and Meth. A 638 (2011) 74.
[14] M. Cavallaro, et al., Nucl. Instr. and Meth. A 637 (2011) 77.
[15] M. Berz, AIP Conf. Proc. 249 (1991) 456.
[16] K. Makino, M. Berz, Nucl. Instr. and Meth. A 427 (1999) 338.
[17] M. Berz, K. Makino, COSY INFINITY, Version 8.1, Department of Physics and Astronomy and NSCL, Michigan State University, East Lansing, USA, 2001.
[18] F. Cappuzzello, et al., Nucl. Instr. and Meth. A 621 (2010) 419.
[19] A. Cunsolo, et al., Nucl. Instr. and Meth. A 484 (2002) 56.
[20] H.A. Enge, Rev. Sci. Instr. 35 (1964) 278.
[21] A. Lazzaro, et al., Nucl. Instr. and Meth. A 570 (2007) 192.
[22] A. Lazzaro, et al., Nucl. Instr. and Meth. A 585 (2008) 136.
[23] A. Lazzaro, et al., Nucl. Instr. and Meth. A 591 (2008) 394.
[24] A. Lazzaro, et al., Nucl. Instr. and Meth. A 602 (2009) 494.
[25] P.M. Endt, et al., Nucl. Phys. A 521 (1990) 1.
[26] G.M. Crawley, G.T. Garvey, Phys. Lett. 19 (1965) 229.
[27] S. Kahana, A.J. Baltz, Adv. in Nucl. Phys. 9 (1977) 1.
[28] N. Anyas-Weiss, et al., Phys. Rep. 13 (no.3) (1974) 201.
[29] W. von Oertzen, A. Vitturi, Rep. Prog. Phys. 64 (2011) 1247.
[30] M. Cavallaro, et al., J. Phys.: Conf. Ser., in press.